Transport in Porous Media **23:** 303–335, 1996.
© 1996 *Kluwer Academic Publishers. Printed in the Netherlands.*

Relative Permeability Relations: A Key Factor for a Drying Model

F. COUTURE[1], W. JOMAA[1] and J.-R. PUIGGALI[2]
[1] *Laboratoire Energétique et Phénomènes de Transfert, Unité de Recherche Associée au CNRS, URA 873, Esplanade des Arts et Métiers, 33405 Talence Cedex, France*
[2] *Laboratoire de Génie des Procédés de Pau – Ecole Nationale Supérieure en Génie des Technologies Industrielles, Rue Jules Ferry, 64000 Pau, France*

(Received: 16 March 1995; in final form: 2 January 1996)

Abstract. In the modelling of heat, mass and momentum transfer phenomena which occur in a capillary porous medium during drying, the liquid and gas flows are usually described by the generalised Darcy laws. Nevertheless, the question of how to determine experimentally the relative permeability relations remains unanswered for most materials that consist of water and humid air, and as a result, arbitrary functions are used in the drying codes. In this paper, the emphasis is on deducing from both numerical and experimental studies a method for estimating pertinent relations for these key parameters. In the first part, the sensitivity of liquid velocity and, consequently, of drying kinetics in the variation of the relative permeabilities is investigated numerically by testing various forms. It is concluded that in order to predict a realistic liquid velocity behaviour, relative permeabilities can be linked to a measurable quantity: the capillary pressure. An estimation technique, based on simulations coupled with experimental measurements of capillary pressure, together with moisture content kinetics obtained for low or middle temperature convective drying, is deduced. In the second part, the proposed methodology is applied to pine wood. It is shown that the obtained relations provide closer representation of physical reality than those commonly used.

Key words: capillary pressure, drying, liquid velocity, modelling, relative permeability.

Nomenclature

AV	averaging volume
$(\mathrm{AV})_j$	j phase volume within the averaging volume AV
a_w	water activity
B_f	resistance factor in the effective diffusitivity coefficient of vapour in the medium
C	mass fraction of the vapour in the gaseous phase
C_p	constant pressure heat capacity [J kg^{-1} K^{-1}]
D	diffusivity [m^2 s^{-1}]
D.C.	convective drying condition assumed to remain constant during the overall process
F_m	total moisture mass flux [kg m^{-2} s^{-1}]
g	gravity vector [m s^{-2}]
h_a	intrinsic averaged enthalpy of dry air [J kg^{-1}]: $h_a = Cp_a(\bar{T} - T_r)$
h_b	specific averaged enthalpy of bound water [J kg^{-1}]: $h_b = h_l - H_b$
$\bar{h}_b$	intrinsic averaged enthalpy of bound water [J kg^{-1}]:

$$\bar{h}_b = h_l - \frac{1}{\bar{\rho}_b}\int_0^{\bar{\rho}_b} H_b d(\bar{\rho}_b)$$

h_l intrinsic averaged enthalpy of free water [J kg^{-1}]: $h_l = Cp_l(\bar{T} - T_r)$
h_s intrinsic averaged enthalpy of solid [J kg^{-1}]: $h_s = Cp_s(\bar{T} - T_r)$
h_v intrinsic averaged enthalpy of vapour [J kg^{-1}]: $h_v = H_v^0 + Cp_v(\bar{T} - T_r)$
H_b heat of desorption [J kg^{-1}]
H_v^0 latent heat of vaporisation at the reference temperature T_r[J kg^{-1}]
I.C. Initial conditions of the medium
J flux
k intrinsic permeability [m^2]
K volumetric mass rate of evaporation [kg m^{-3} s^{-1}]
k_r relative permeability
L thickness of the medium [m]
n exterior normal unit vector
P pressure [Pa]
q source term
Q total heat flux [W m^{-2}]
RH external relative humidity [%]
T temperature [K or °C]
T_{infh} wet bulb temperature [K or °C]
T_r reference temperature [K]: $T_r = 273.16$ K
t time [s]
S saturation
U conserved quantity
V velocity [m s^{-1}]
W moisture content (in dry basis)
z space variable [m]

Greek Symbols
δz space step [m]
ϵ porosity
ε_j volume fraction for the phase j: $\varepsilon_j = (\text{AV})_j/\text{AV}$
Φ heat source [W m^{-3}]
λ effective thermal conductivity [W m^{-1} K^{-1}]
μ dynamic viscosity [kg m^{-1} s^{-1}]
ρ density [kg m^{-3}]
τ_m mass transfer coefficient [m s^{-1}]
τ_T heat transfer coefficient [W m^{-2} K^{-1}]
σ surface tension [N m^{-1}]

Subscripts
a dry air
atm atmospheric
b bound water
c capillary
eq equilibrium
g gas
inf drying air
ini initial
irr irreducible
l liquid
m macroscopic mean value
s solid
ssp solid saturation point
v vapour
vsat saturate vapour

Mathematical Operators

$-$ average value of a quantity Ψ:

$$\bar{\Psi} = \frac{1}{\mathrm{AV}} \int_{\mathrm{AV}} \Psi d(\mathrm{AV})$$

$-j$ intrinsic average over the phase j of a quantity Ψ:

$$\bar{\Psi}^j = \frac{1}{(\mathrm{AV})_j} \int_{\mathrm{AV}} \Psi d(\mathrm{AV})$$

∇ gradient operator

$\nabla\cdot$ divergence operator

1. Introduction

The mathematical description of the physics involved during the drying of a hygroscopic capillary porous medium has been discussed by numerous authors. Most of them adopt a continuum approach based on Whitaker's theory (1977), where the macroscopic partial differential equations are achieved by volume averaging the microscopic conservation laws. The value of any physical quantity at a point in space is given by its average value on the averaging volume (AV) centred on this point.

Within each AV (circle in Figure 1), the porous medium consists of:

- a continuous solid phase which contains incompressible solid structure assumed rigid together with hygroscopically held bound water (bound water is negligible for nonhygroscopic media),
- a liquid phase (free water) assumed incompressible,
- a continuous gas phase supposed to be a perfect mixture of vapour and dry air, considered as ideal gases.

The total moisture (free water + bound water + vapour) is usually represented by the moisture content W, defined in dry basis reference by

$$W = (\bar{\rho}_l + \bar{\rho}_v + \bar{\rho}_b)/\bar{\rho}_s, \tag{1}$$

with the notations listed at the beginning of the paper. A relevant parameter is associated with each moisture type

- for the bound water, the bound moisture content W_b,

$$W_b = \bar{\rho}_b/\bar{\rho}_s; \tag{2}$$

- for the free water, the saturation S,

$$S = \frac{\varepsilon_l}{\varepsilon} = \frac{\bar{\rho}_s(W - W_b) - \varepsilon\bar{\rho}_v^g}{\varepsilon\bar{\rho}_l^l - \varepsilon\bar{\rho}_v^g}, \tag{3}$$

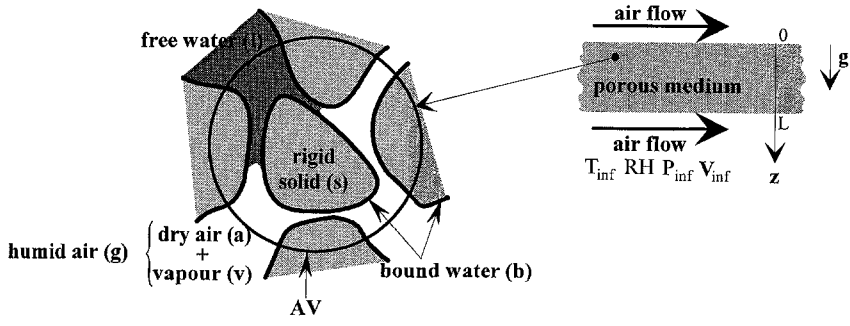

Figure 1. Components of hygroscopic capillary porous medium, averaging volume and drying configuration considered in this work.

where ε is the porosity and ε_l the volume fraction for the liquid phase within the AV;

- for the vapour, the mass fraction in the gas phase C,

$$C = \bar{\rho}_v / \bar{\rho}_g. \tag{4}$$

The successive stages in the removal of moisture at a point of the medium during the overall drying process are schematised in Figure 2. There are two main regions depending on the state (free or bound) of the water present in the AV.

- *Region I*: in this region, called the *nonhygroscopic region*, free water exists within the AV ($1 > S > 0$) and the solid phase is fully saturated with bound water. The transition point between the regions I and II is reached when all free water has been removed from the AV and the solid phase remains fully saturated with bound water. This point is known as the solid saturation point (ssp) ($S = 0$ or $W = W_{ssp}$). Some authors divide the nonhygroscopic region into two parts by using the concept of the irreducible saturation point ($S = S_{irr}$ or $W = W_{irr}$) with the view that above that level the liquid phase is continuous (*region Ia* called *funicular region*) and discontinuous below it (*region Ib* called *pendular region*) (Spolek and Plumb, 1981; Whitaker and Chou, 1983–84; Kaviany and Mittal, 1987; Perré and Moyne, 1991; Puiggali and Quintard, 1992). Nevertheless and especially for hygroscopic media, others prefer to assume that free water exists in only the funicular state above the solid saturation point (Perré and Degiovanni, 1990; Ferguson and Turner, 1994).
- *Region II*: in this region, called *hygroscopic region*, only bound water remains in the AV.

The process ends when the value of the equilibrium moisture content W_{eq}, dictated by the drying conditions, is reached throughout the medium.

The hypothesis and the way to obtain the governing equations for heat and mass transports during drying have been well established and are not discussed here. As the reader can find the finer developments in the previous references, only the relevant set of macroscopic partial differential equations is summarised below, all the necessary notations being given in the nomenclature. Within the framework of this paper, only a one-dimensional modelling is used. The complete differential form of the conservation laws for the mass of each component of the medium and for energy is summarised as follows:

$$\frac{\partial U}{\partial t} + \nabla \cdot \mathbf{J} = q, \tag{5}$$

with for solid: $U = \bar{\rho}_s, \quad \mathbf{J} = 0, \quad q = 0,$

for dry air: $U = \bar{\rho}_a, \quad \mathbf{J} = \bar{\rho}_a^g \bar{\mathbf{V}}_a, \quad q = 0,$

for vapour : $U = \bar{\rho}_v, \quad \mathbf{J} = \bar{\rho}_v^g \bar{\mathbf{V}}_v, \quad q = K_l + K_b,$

for free water: $U = \bar{\rho}_l, \quad \mathbf{J} = \bar{\rho}_l^l \bar{\mathbf{V}}_l, \quad q = -K_l,$

for bound water: $U = \bar{\rho}_b \quad \mathbf{J} = \overline{\rho_b \mathbf{V}_b}, \quad q = -K_b,$

for energy :

$$U = \bar{\rho}_s h_s + \bar{\rho}_a h_a + \bar{\rho}_v h_v + \bar{\rho}_l h_l + \bar{\rho}_b \bar{h}_b,$$

$$\mathbf{J} = \bar{\rho}_a^g \bar{\mathbf{V}}_a h_a + \bar{\rho}_v^g \bar{\mathbf{V}}_v h_v + \bar{\rho}_l^l \bar{\mathbf{V}}_l h_l + \overline{\rho_b \mathbf{V}_b} h_b - \lambda \cdot \nabla \bar{T}, \quad q = \Phi.$$

The mass flux expressions are indicated in Figure 2 together with the classical migration mechanisms. In the funicular region, the convective liquid flow which arises due to capillarity, an internal gaseous pressure gradient and gravity is described by the generalised Darcy's law. In the hygroscopic region, a diffusive mechanism driven by a bound moisture content gradient allows the bound water migration. For vapour and dry air, the phenomena are the same during the overall drying process: convection by gas flow defined by Darcy's law and diffusion in the medium given by Fick's law. In writing the energy conservation equation, the following hypothesis are made:

- according to Turner and Bremhorst (1994), an enthalpy formulation over a complete energy formulation is sufficient;
- a local thermal equilibrium exists between the solid, the gas and the liquid phases, i.e. the temperatures for the three phases are the same (Whitaker, 1991; Quintard and Whitaker, 1993).

The mathematical modelling is closed by the commonly used assumption that the partial pressure of vapour is equal to its equilibrium value

$$\bar{P}_v^g = \begin{cases} P_{\text{vsat}} & \text{if } W \geqslant W_{\text{ssp}}, \\ a_w P_{\text{vsat}} & \text{if } W < W_{\text{ssp}}, \end{cases} \tag{6}$$

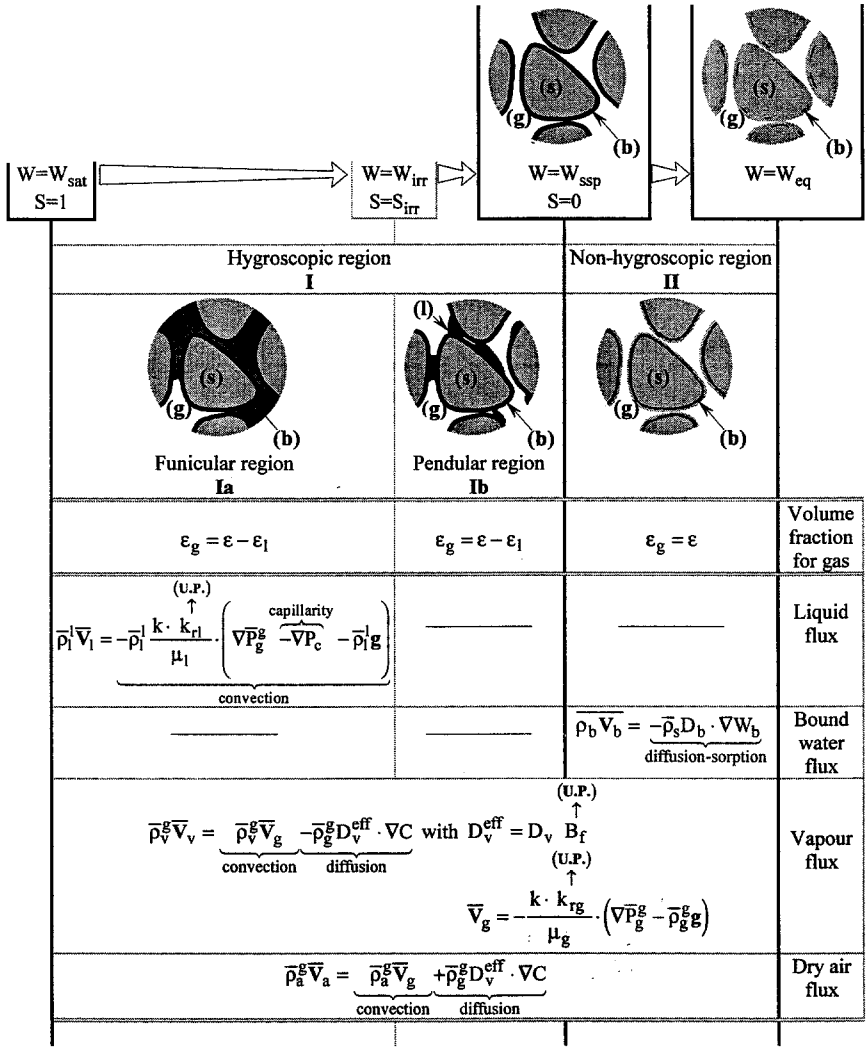

Figure 2. Successive stages in the removal of moisture during drying and corresponding mass flux models. The parameters marked by UP remain unknown.

where a_w is the water activity and P_{vsat} the saturation vapour pressure.

At this stage two main difficulties are encountered to pass from the modelling to realistic simulations. The first concerns the problems involved in the numerical resolution of a highly nonlinear and strongly coupled set of equations. This point is dealt with in numerous works: for example, one-dimensional codes can be found in (Plumb *et al.*, 1985; Stanish *et al.*, 1986; Puiggali and Quintard, 1986, 1992; Perré, 1987a; Moyne, 1987; Turner and Ilic, 1990; Rogers and Kaviany,

Table I. Measurable parameters of a complete drying modelling.

Parameters	Examples of experimental methods
Porosity (ε)	High pressure mercury porosimeter (Tsakiroglou *et al.* 1990)
Dry solid density ($\bar{\rho}_s$)	Densitometric analysis, (Kanowsky 1985)
Intrinsic permeability (k)	Flow rate by pressure difference (Perré, 1987b)
Water activity (a_w)	Salt saturated solutions (Bizot *et al.*, 1987)
Bound water diffusivity (D_b)	Steady-state method (Choong, 1965)
Effective thermal conductivity (λ)	Flash method (Gobbé and Gounot, 1991)
Capillary pressure (P_c)	High pressure mercury porosimeter (Spolek and Plumb, 1981)

1992) and more recently, two-dimensional resolutions have been implemented by Perré and Degiovanni (1990), Ouelhazi *et al.* (1992), Fyhr and Rasmuson (1994), Turner (1994), Boukadida and Ben Nasrallah (1995) or Couture (1995). The second difficulty is linked to the knowledge of the physical parameters needed for the simulation of a complex hygroscopic capillary porous medium drying. Although a relatively large number of these parameters are obtained with some confidence by experiments in which a 'single' phenomenon can be identified (see Table I), the question of how to determine experimentally the effective diffusivity coefficient of vapour in the medium (D_v^{eff}) and the relative permeabilities (k_{rl} and k_{rg}) for two coexistent fluids such as water liquid and humid air still remains unanswered. Thus, except for some ideal materials for which geometrical considerations can be made, the correlating functions used for these three quantities result from an arbitrary choice. To highlight the importance of this choice, unknown parameters are marked by (UP) in Figure 2: it should be noted that these parameters can influence substantially the total moisture transport in the nonhygroscopic region.

In this paper the emphasis is on deducing from both numerical and experimental studies, a method for determining pertinent relations for the relative permeabilities. The effective diffusivity coefficient of vapour is taken as a valid datum and is not discussed here.

The form of the relative permeability relations depends on the existence, or not, of a pendular region. The irreducible saturation concept is first analysed from works available in the literature and, finally is ruled out. This leads to the assumption that the liquid phase remains continuous during the overall nonhygroscopic region, so that the relevant physical behaviour for the liquid flux is to decrease to a null value as the moisture content reaches the solid saturation point. In order to provide k_r relations which ensure this behaviour, the sensitivity of liquid velocity and moisture content profiles in relative permeabilities is investigated numerically. The physical configuration considered is low or middle temperature convective drying of pine wood (see Figure 1). Both the process and the material have been chosen for the following two main reasons.

- For pine wood, the measurable parameters which are listed in Table I have been well identified in the past for temperatures in the range of 0 and 100°C (Lartigue and Puiggali, 1987; Bonneau, 1991).
- For convective drying, closure of the system by boundary conditions can be obtained accurately by using the boundary-layer theory and the classical Lewis analogy:

$$\bar{P}_g^g = P_{\text{atm}}, \tag{7}$$

$$(\rho_l \bar{\mathbf{V}}_l + \bar{\rho}_v^g \bar{\mathbf{V}}_v + \overline{\rho_b \mathbf{V}_b}) \cdot \mathbf{n} = F_m, \tag{8}$$

$$(\bar{\rho}_a^g \bar{\mathbf{V}}_a h_a + \bar{\rho}_v^g \bar{\mathbf{V}}_v h_v + \bar{\rho}_l^l \bar{\mathbf{V}}_l h_l + \overline{\rho_b \mathbf{V}_b} h_b - \lambda \cdot \nabla \bar{T}) \cdot \mathbf{n}$$
$$= (\bar{\rho}_a^g \bar{\mathbf{V}}_a h_a) \cdot \mathbf{n} + F_m h_v + Q, \tag{9}$$

where the total moisture mass flux F_m and the total heat flux Q are defined by

$$F_m = \tau_m(\bar{\rho}_v^g - \rho_{v_{\text{inf}}}), \tag{10}$$

$$Q = \tau_T(\bar{T} - T_{\text{inf}}), \tag{11}$$

the quantities τ_m and τ_T being the mass transfer and heat transfer coefficients, respectively.

In order to assist with the vocabulary used throughout this text, it could be useful to remember succinctly the mean characteristics of the successive convective drying periods.

- *Initial transient period*: during this short period, the temperature quickly rises until it reaches the wet bulb temperature, which is determined by the external air conditions, throughout the medium.
- *Constant rate period*: this period is defined by a constant drying rate. All the medium is in the funicular region, so that internal capillary forces provide the continuous supply of liquid to the surfaces where all the energy transferred is used directly for evaporation. The temperature remains at the wet bulb temperature.
- *Falling rate period*: under the assumption that a pendular region does not exist, the drying rate begins to fall as the surfaces reach the hygroscopic region. An evaporation zone recedes inwards through the material and as a result, the temperature increases toward the external temperature.

The simulations are performed by employing the one-dimensional code which has been developed from system (5) in previous work (Couture *et al.*, 1995). The interested reader is referred to that paper for details concerning the resolution.

It is concluded from the numerical study carried out in this paper that the relative permeabilities, which are unknown key model parameters, can be linked

to a measurable quantity: the capillary pressure. Finally, a method for predicting these parameters using both simulations and experiments is proposed and applied to pine wood.

2. Methodology for Estimating Relative Permeabilities

In many disciplines, the modelling of coupled two phase flow in porous media is derived from the extension of Darcy's law to multiphase flow by introducing the relative permeability concept:

$$\bar{\mathbf{V}}_j = -\frac{k \cdot k_{rj}}{\mu_j} \cdot (\nabla \bar{P}_j^j - \bar{\rho}_j^j \mathbf{g}), \tag{12}$$

where j designates the jth phase, k_{rj} being the relative permeability of phase j. Although a consensus does not exist concerning the impact of the flow situation on the relative permeability (for example, countercurrent-flow or cocurrent-flow), k_{rj} is commonly specified as a function of saturation alone. In this work, given the existing knowledge, this hypothesis is accepted.

Due to the difficulties in measuring relative permeability, techniques for obtaining the constitutive relations for this quantity have been examined extensively in soil science and petroleum engineering. Many methods for estimating k_{rj} as a function of saturation have been proposed and can be divided into two groups: those based on capillary pressure measurements and those whose functional form is a power function of saturation. A review of these methods can be found in (Hornapour *et al.*, 1986). However, the circumstances encountered in drying totally differ from those covered by soil science or petroleum engineering, so that the available techniques cannot be applied within the framework of classical drying problems. Indeed, the saturation to which the relative permeability corresponds must be measured and one of the important assumptions on which the approaches are based is that no mass transfer between the phases occurs during the experiment. Although well verified for two coexistent immiscible fluids such as oil-water, oil-gas or water-gas, with the gas being non humid air in the last case, this assumption is not valid for the two phases considered in drying: water and humid air. The measured saturation, essentially at low humidity levels, depends on the thermodynamical equilibrium between the two fluids. To highlight the difficulties raised by the coexistent phases of water and humid air, one can note that the only experimental data concerning the relative permeabilities of wood, which is a porous material broadly discussed in the drying literature, are available for water-oil or water-nitrogen systems (Tesoro *et al.*, 1972, 1974).

Due to this problem, for most of the porous media that consist of water and humid air, the relative permeabilities remain unknown experimentally, and consequently arbitrary functions must be used within the infrastructure of the drying codes. The first part of this paper focuses on proposing an estimation technique, based

on experimental measurements of both moisture content (related to saturation by Equation (3)) during convective drying and capillary pressure.

2.1. THE IRREDUCIBLE SATURATION CONCEPT

A review of the drying literature indicates that two types of functions of saturation S, depending on a pendular region existing, or not (*region Ib* in Figure 2), are commonly used for the relative permeabilities k_{rl} and k_{rg}. The range of variation of the capillary pressure P_c, defined by

$$P_c = \bar{P}_g^g - \bar{P}_l^l, \tag{13}$$

changes accordingly. In all cases, this parameter is obtained by either correlating measured data (Whitaker, 1984; Bonneau, 1991; Puiggali and Quintard, 1992) or using geometrical models such as Comstok model (Plumb *et al.*, 1985; Perré, 1987a). It is assumed to depend on saturation and temperature as follows:

$$P_c(S, \bar{T}) = P_{cs}(S)\sigma(\bar{T}). \tag{14}$$

By taking into account an irreducible saturation level S_{irr}, the liquid phase continuity is disrupted when the saturation falls below S_{irr}, so that liquid flow is no longer possible. This behaviour is described by introducing a k_r model which can be represented as follows (Spolek and Plumb, 1981; Whitaker and Chou, 1983–84; Kaviany and Mittal, 1987; Perré and Moyne, 1991; Puiggali and Quintard, 1992)

$$\begin{aligned} &\text{for } S > S_{irr} \quad k_{rl} = \left\{\frac{(S - S_{irr})}{(1 - S_{irr})}\right\}^{\alpha} \quad k_{rg} = \left\{\frac{(1 - S)}{(1 - S_{irr})}\right\}^{\beta}; \\ &\text{for } S \leqslant S_{irr} \quad k_{rl} = 0 \qquad\qquad\qquad\quad k_{rg} = 1, \end{aligned} \tag{15}$$

where α and β are constants. The capillary pressure P_c theoretically tends toward infinity at S_{irr}.

Other authors prefer to assume that the liquid phase remains continuous (funicular state) during the overall nonhygroscopic region, especially for hygroscopic media (Perré and Degiovanni, 1990 for fir; Ferguson and Turner, 1994 for spruce). Then, the liquid flow is extended up to the solid saturation point by using the following form for relative permeabilities

$$\text{whatever } S \qquad k_{rl} = S^{\alpha} \qquad k_{rg} = (1 - S)^{\beta}. \tag{16}$$

The capillary pressure P_c theoretically tends toward infinity at the zero value of S.

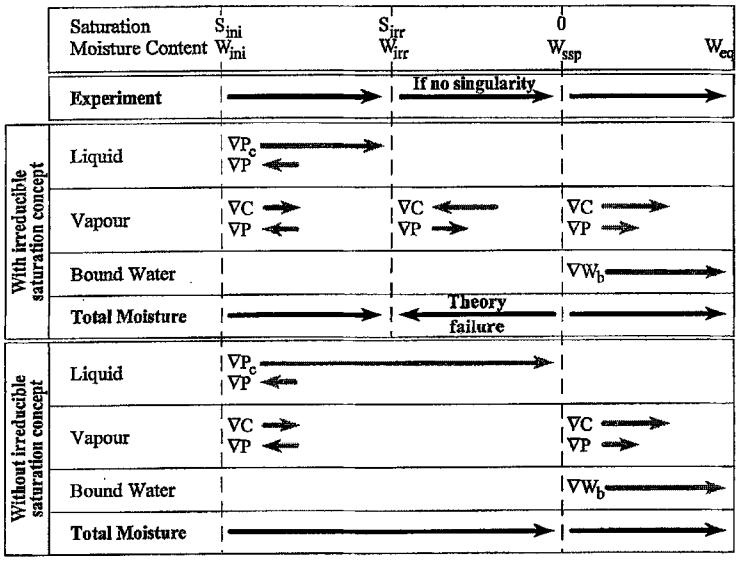

Figure 3. Moisture movements and corresponding driving gradients during the overall drying process with and without the irreducible saturation concept. Arrows directed toward the right indicate a flow toward the surface of the medium.

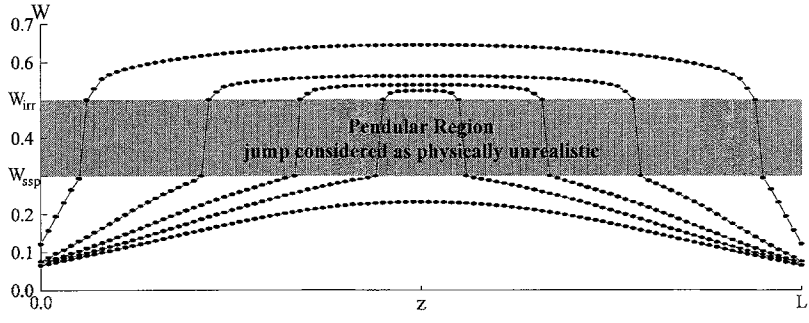

Figure 4. Predicted moisture concent profiles for heartwood of pine by taking into account the irreducible saturation concept. Relative permeabilities are given by Equations (15) with $\alpha = \beta = 3$. The other parameters are listed in Appendices A and B. $L = 2.5$ cm. D.C.: $T_{inf} = 60°C$; RH = 30%; $\tau_T = 12\,W\,m^{-2}\,K^{-1}$; $P_{inf} = P_{atm}$. I.C.: $W = 1$; $T = 25°C$; $P = P_{atm}$.

For the two approaches (with irreducible saturation concept, Equations (15) and without irreducible saturation concept, Equations (16)), Figure 3 shows, in a simplified manner, directions of theoretical moisture flows together with the driving gradient which enable these migrations during convective drying.

2.1.1. *With Irreducible Saturation Concept, Equations* (15)

It obviously results from generalised Darcy's law (12) and Equations (15) that there is no liquid phase transport of moisture in the pendular region [0-S_{irr}]. Moreover, the gas phase diffusive transport of moisture is from the region of high temperature to the region of low temperature. For a classical convective process, this migration is thus directed away from the drying surfaces (∇C in Figure 3). Whitaker (1984) has shown that the gas phase convective transport (∇P in Figure 3) is not enough to overcome the diffusive transport. The author concludes that, in the current theoretical formulation, *there are no mechanisms which allow the moisture transport toward the drying surfaces for saturation between S_{irr} and the solid saturation point.* As a result, the set of equations produces a mathematical singularity (Puiggali and Quintard, 1992): the pendular zone must be replaced by a jump in the saturation on the order of S_{irr}. A steep front in the predicted moisture profiles recedes inwards through the material.

After examining several drying experiments which have been carried out for nonhygroscopic media (Cunningham and Kelly, 1978 for glass beads and Recan, 1982 for a sand layer), Moyne (1987) confirmed that the solution resides in a pendular zone reduced to a jump. A 'drying front' modelling was proposed and implemented by the author, but only in the simplified case of a description based on a single diffusion equation for saturation. Moreover, the physical reality of a jump is not accepted unanimously.

2.1.2. *Without Irreducible Saturation Concept, Equations* (16)

The experimental data of Ceaglske and Hougen (1937) for a sand layer illustrate the existence of a continuous moisture flux toward the surfaces between S_{irr} and zero. On the basis of these results and in order to remove the inconsistency of the theory, Whitaker (1984) puts forward the following assumption: some liquid phase mass transport occurs in this region. Thus, capillary pressure and relative permeability are extended to a saturation point near zero by introducing a new value for S_{irr}. However, in order to match computed and measured values, the film heat transfer coefficient is adjusted in such a way that the traditional heat and mass transfer analogy is not verified.

The use of Equations (16) for the relative permeabilities leads to the same hypothesis as that made by Whitaker: the pendular zone does not exist and moisture transport toward the surfaces is ensured by capillarity until the solid saturation point is reached (∇P_c in Figure 3).

2.1.3. *Theory Adopted in this Work*

The mathematical singularity induced by the irreducible saturation point appears to a slight extent physically unrealistic. For example, concerning oak and heartwood of pine (two hygroscopic materials), values of about 0.5 and 0.25 respectively for

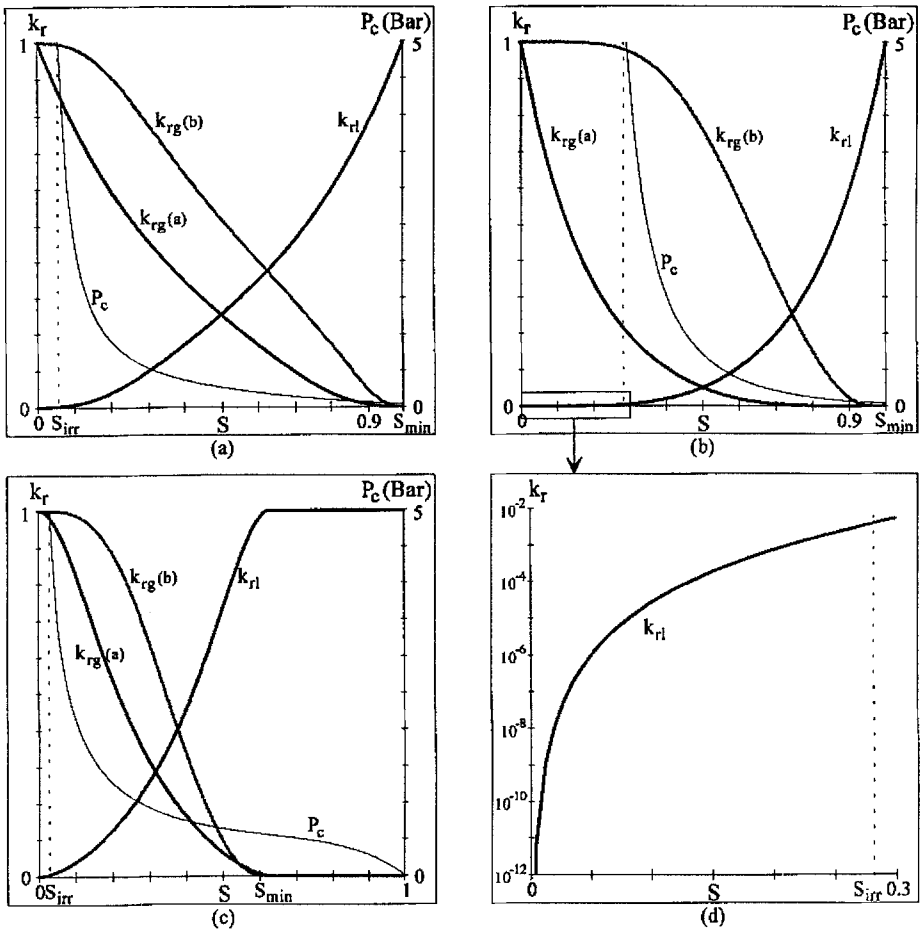

Figure 5. Relative permeabilities versus saturation given by Equations (27), (28a) and (28b) with $f(S) = 1$ for a representative set of experimental capillary pressure curves (see Appendix A). The media are sapwood (a), heartwood (b), (d) and late wood (c) of pine.

S_{irr} are reported (Hernandez, 1991; Bonneau, 1991), so that the numerical code produces moisture content profiles displaying a jump which seems excessively large, as illustrated for heartwood of pine in Figure 4. To our knowledge, there are no experimental studies undertaken on hygroscopic media which has shown the existence of a front between $W_{irr}(\Leftrightarrow S_{irr})$ and $W_{ssp}(\Leftrightarrow S = 0)$. This fact is accentuated by the measurements on sapwood of pine ($S_{irr} = 0.07 \Leftrightarrow W_{irr} = 0.4$; $W_{ssp} = 0.3$) proposed in the last part of the paper. Although experiment does not provided indisputable proof, in so far as measure gives necessarily averaged values and it is possible for local heterogeneities or three-dimensional transports to cause

case	1	2	3	4	5	6
$k_{rl}(S)$	$S^{1.5}$	S^2	Equation (27) f(S) = 1	Equation (27) f(S) = 1	$S^{2.5}$	S^3
$k_{rg}(S)$	$(1\text{-}S)^{1.5}$	$(1\text{-}S)^2$	Equation (28a) f(S) = 1	Equation (28b) f(S) = 1	$(1\text{-}S)^{2.5}$	$(1\text{-}S)^3$

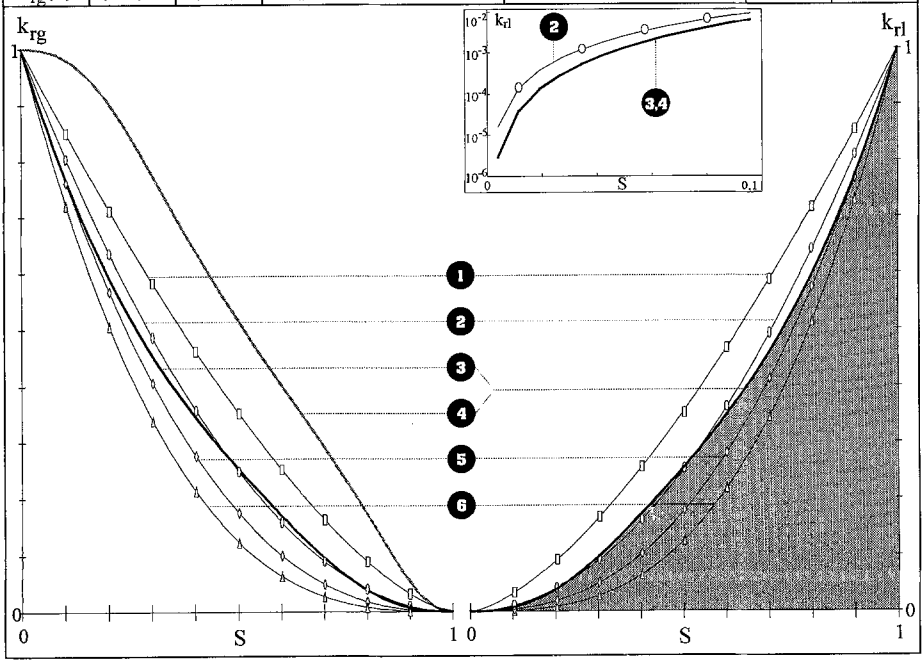

Figure 6. Relative permeabilities versus saturation for the six test cases of the numerical study. The shaded area indicates the liquid relative permeability values which ensure a realistic behaviour for the liquid velocity.

real one-dimensional jumps to flatten, it remains the only available representation of the physical reality. Since the purpose of any modelling work must be to describe this reality (i.e. the experimental behaviour), we assume that *the pendular region* $[0\text{-}S_{irr}]$ *cannot be reduced to a front.*

Under this assumption, two possibilities can be considered.

- *A pendular region exists.* In this region, the mathematical formulation given in the introduction is not able to correctly describe the physics: *a new modelling is needed* in order to ensure moisture migration toward the drying surfaces.
- *The current modelling* based on the generalised Darcy's law *is accepted.* In order to remove the failure of the theory raised by Whitaker (1984), a liquid flow must occur in the region $[0\text{-}S_{irr}]$. To achieve this behaviour, the liquid relative permeability function must induce flow until the solid saturation point $(S = 0)$ is reached, in a similar manner as those represented by Equations (16). The only available theoretical basis is that the liquid phase is continuous during the overall non-hygroscopic zone, i.e. *the pendular region does not*

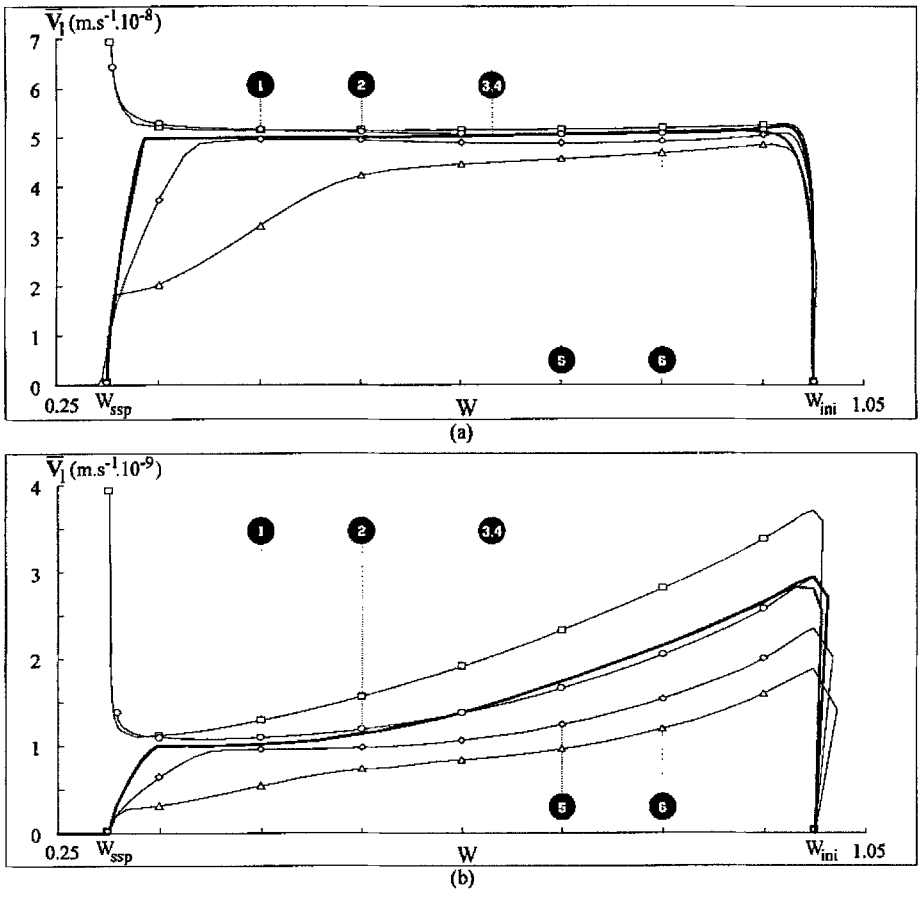

Figure 7. Predicted liquid velocity versus moisture content curves by using the six relative permeability relations given in Figure 6: (a) at the quarter point ($z = 3L/4$) and (b) near the centre ($z = L/2 + \delta z/2$) of the medium. $L = 2.5$ cm. D.C.: $T_{inf} = 60°C$; RH $= 30\%$; $\tau_T = 12\,W\,m^{-2}\,K^{-1}$; $P_{inf} = P_{atm}$. I.C.: $W = 1$; $T = 25°C$; $P = P_{atm}$.

exist. Although this postulate is currently used (see Equations (16)), it must be underlined that it remains an hypothesis which is unverified experimentally. However, for hygroscopic media, one can imagine that a thin film of water bound to the internal walls could ensure the continuity.

Here, the study of relative permeabilities is undertaken within the framework of the common modelling described previously, so that the second possibility is adopted. Subsequently, relations based on the following properties are investigated.

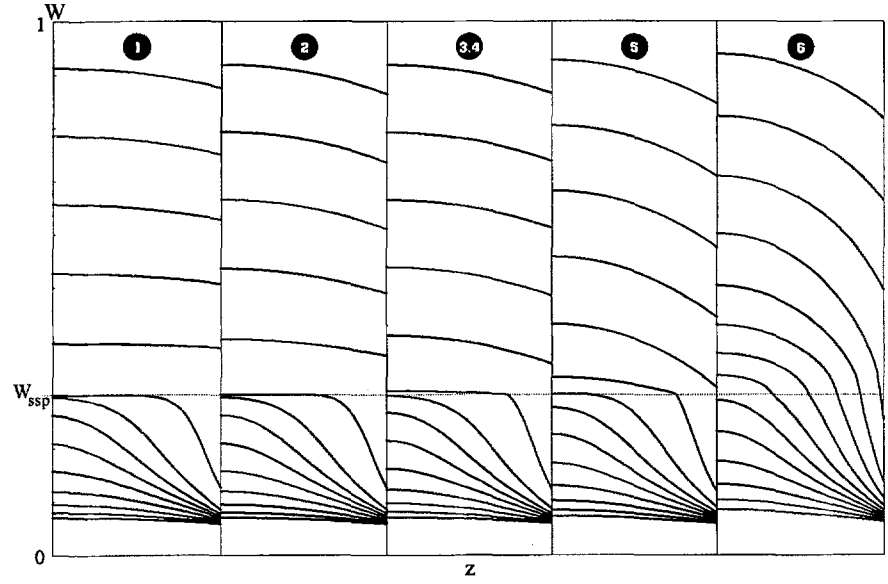

Figure 8. Predicted moisture content profiles every two hours by using the six relative permeability relations given in Figure 6. $L = 2.5$ cm. D.C.: $T_{inf} = 60°C$; RH = 30%; $\tau_T = 12$ W m^{-2} K^{-1}; $P_{inf} = P_{atm}$. I.C.: $W = 1$; $T = 25°C$; $P = P_{atm}$.

P[1] Liquid and gas phase relative permeabilities: **a**- are expressed as functions of saturation alone; **b**- decrease and increase, respectively, as S decreases; **c**- verify:

$$\lim_{S\to 1} k_{rl}(S) = 1; \qquad \lim_{S\to 0} k_{rl}(S) = 0; \tag{17a,b}$$

$$\lim_{S\to 1} k_{rg}(S) = 0; \qquad \lim_{S\to 0} k_{rg}(S) = 1. \tag{18a,b}$$

P[2] Capillary pressure: **a**- depends on S as indicated by Equation (14); **b**- increases indefinitely as S tends toward zero:

$$\lim_{S\to 0} P_c(S, \bar{T}) = +\infty. \tag{19}$$

P[3] By ruling out the irreducible saturation concept, the relevant physical behaviour for the liquid flux during a classical convective drying process is, **a**- except during a short initial transient period, to decrease with S within the overall non-hygroscopic region; **b**- to tend toward zero as the moisture content reaches the solid saturation point ($S = 0$):

$$\lim_{S\to 0} \bar{\mathbf{V}}_l = \mathbf{0}. \tag{20}$$

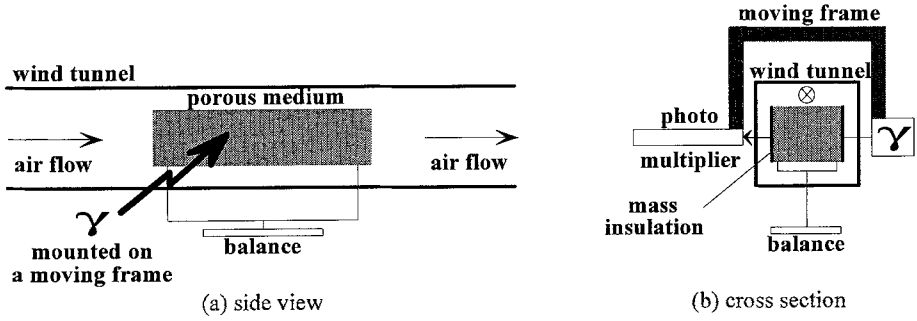

Figure 9. Experimental set-up.

2.2. A LINK TO THE CAPILLARY PRESSURE

For low or middle temperature convective drying, except during the initial transient period, the most important part of the liquid flow results from capillary forces. As a result, the evolutions of liquid velocity are directly linked to the variations of the capillary pressure gradient. By introducing Equations (13) into the generalised Darcy's law (12) and by neglecting the liquid transport owing to total gas phase pressure gradients and temperature gradients, this link can be described by the following approximation:

$$\bar{\mathbf{V}}_l \approx \frac{k}{\mu_l(\bar{T})} k_{rl}(S) \frac{\partial P_c}{\partial S}(S, \bar{T}) \nabla S. \tag{21}$$

The limit as S tends toward zero is given by

$$\lim_{S \to 0} \bar{\mathbf{V}}_l \approx \frac{k}{\mu_l(\bar{T})} \times \lim_{S \to 0} k_{rl}(S) \times \lim_{S \to 0} \frac{\partial P_c}{\partial S}(S, \bar{T}) \times \lim_{S \to 0} \nabla S. \tag{22}$$

As previously mentioned, a jump in the saturation profiles is prohibited so that the absolute value of ∇S remains lower than a finite value. Let ∇S_0 be the finite limit of ∇S as S approaches 0. According to Equations (17b) and (19) associated with properties $\mathbf{P}^1\mathbf{c}$ and $\mathbf{P}^2\mathbf{b}$, respectively, Equation (22) gives

$$\lim_{S \to 0} \bar{\mathbf{V}}_l \approx \frac{k}{\mu_l(\bar{T})} \times (0) \times (-\infty) \times (-\mathrm{FV} \leqslant \nabla S_0 \leqslant \mathrm{FV})$$

with FV representing some finite value. (23)

In order to ensure property $\mathbf{P}^3\mathbf{b}$ (Equation (20)), the indeterminate raised by the product $(0) \times (-\infty)$ must be removed. This can be achieved by relating the relative

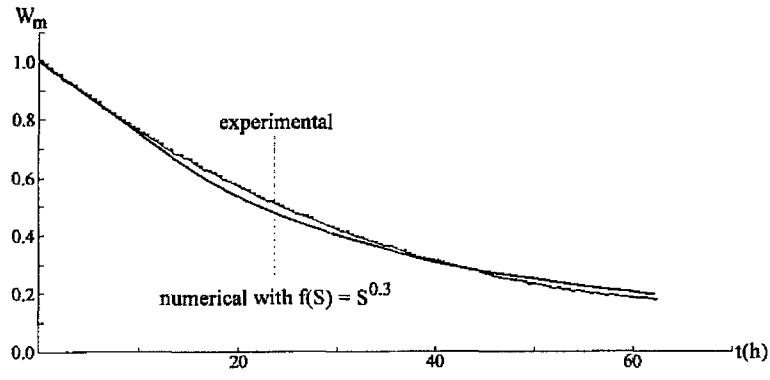

Figure 10. Adjustment of $f(S)$ from Exp. 1: comparison of experimental and predicted drying kinetics. $L = 7$ cm. D.C.: $T_{\text{inf}} = 70°\text{C}$; RH = 20%; $\tau_T = 9.8\,\text{W m}^{-2}\,\text{K}^{-1}$; $P_{\text{inf}} = P_{\text{atm}}$. I.C.: $W =$ experimental profile at $t = 00{:}00{:}00$ (see Figure 11); $T = T_{\text{infh}} = 39.7°\text{C}$; $P = P_{\text{atm}}$.

permeability of the liquid phase to the partial derivative of the capillary pressure with respect to the saturation as follows

$$k_{rl}(S) = f(S)\left(\min_{S<s<1}\left|\frac{\partial P_c}{\partial S}(s,\bar{T})\right| \Big/ \left|\frac{\partial P_c}{\partial S}(S,\bar{T})\right|\right). \tag{24}$$

Indeed, by substituting for k_{rl} from this relation into Equation (21), it may be seen that it is sufficient to impose that

$$\lim_{S\to 0} f(S) = 0, \tag{25}$$

to obtain property $\mathbf{P^3b}$:

$$\begin{aligned}\lim_{S\to 0} \bar{\mathbf{V}}_l &\approx \frac{k}{\mu_l(\bar{T})} \times \lim_{S\to 0} f(S) \times \min_{S<s<1}\left|\frac{\partial P_c}{\partial S}(S,\bar{T})\right| \times (\pm 1) \times \nabla S_0 \\ &= \lim_{S\to 0} f(S) = 0.\end{aligned} \tag{26}$$

This leads us to propose the following functions of the saturation for relative permeabilities, those given for gas phase being deduced from the liquid phase relation by symmetrical considerations

$$k_{rl}(S) = f(S)\left(\min_{S<s<1}\left|\frac{\partial P_c}{\partial S}(s)\right| \Big/ \left|\frac{\partial P_c}{\partial S}(S)\right|\right); \tag{27}$$

$$k_{rg}(S) = f(1-S)\frac{\min_{S<s<1}\left|\frac{\partial P_c}{\partial S}(s)\right|}{\left|\frac{\partial P_c}{\partial S}(S_{\min} - S)\right|} \quad \text{or}$$

$$k_{rg}(S) = f(1-S)\frac{\min_{S<s<1}\left|\frac{\partial P_c}{\partial S}(s)\right|}{\left|\frac{\partial P_c}{\partial S}(S_{\min}(1-k_{rl}(S)))\right|}; \qquad (28a,b)$$

$f(S)$ being positive and $S_{\min}$ being defined by

$$\left|\frac{\partial P_c}{\partial S}(S_{\min})\right| = \min_{S<s<1}\left|\frac{\partial P_c}{\partial S}(s)\right|.$$

It should be noted that in the partial derivative of P_c with respect to S, temperature has been omitted, willingly, in order to show that the proposed expressions depend only on saturation ($\mathbf{P^1a}$). Indeed, by developing $(\partial P_c/\partial S)$ from Equation (14) ($\mathbf{P^2a}$) in Equation (24), surface tension σ appears in both the numerator and the denominator, so that terms due to temperature vanish.

In the above relations, the factor $f(S)$ is expected to be an intrinsic parameter which is adjustable in the range defined by properties $\mathbf{P^1}$ to $\mathbf{P^3}$ in such a way that modelling provides a close representation of physical reality. The next section deals with the conditions required for $f(S)$, together with its estimation.

2.3. PROPERTIES AND ESTIMATION OF $f(S)$

As a starting point, consider the case $\mathbf{f(S) = 1}$. The resulting forms of $k_{rl}(S)$ and $k_{rg}(S)$ are shown in Figure 5 for three correlating functions of capillary pressure, experimentally determined by Bonneau (1991). These three cases have been selected to cover the different capillary pressure shapes commonly reported in the literature, the two main differences being the existence of an inflection point $S_{\min}$ due to a steep slope at $S = 1$ (Figure 5(c) as compared with Figures 5(a) and 5(b)), and the saturation level where the slope of the curves rises drastically. In fact this level, which is represented as a thin dotted line, corresponds to the irreducible saturation point S_{irr} when it is taken into account. Note that although the capillary pressure curves are truncated in order to allow the graphical representations, the functions given by Bonneau tend toward infinity as the saturation approaches zero according to property $\mathbf{P^2b}$ (see Appendix A). Analysis of the graphs indicates that the overall trends of the relative permeability curves are in good agreement with the usual forms encountered in the literature, and satisfy property $\mathbf{P^1}$. Moreover, for saturations lower than the 'old irreducible point', the liquid relative permeability is difficult to distinguish from zero (Figure 5(b)) but remains nonzero (Figure 5(d)), as recommended by Whitaker (1984) in order to ensure the liquid flux continuity previously discussed.

The parameter $f(S)$ is required to preserve the general shapes displayed in Figure 5, so that now some conditions related to property $\mathbf{P^1}$ could be put forward. Nevertheless, before any definite conclusions can be draw, an investigation of property $\mathbf{P^3}$ associated with the liquid velocity behaviour is needed, especially concerning $\mathbf{P^3a}$ because $\mathbf{P^3b}$ were discussed in section 2.2 (Equation (25)).

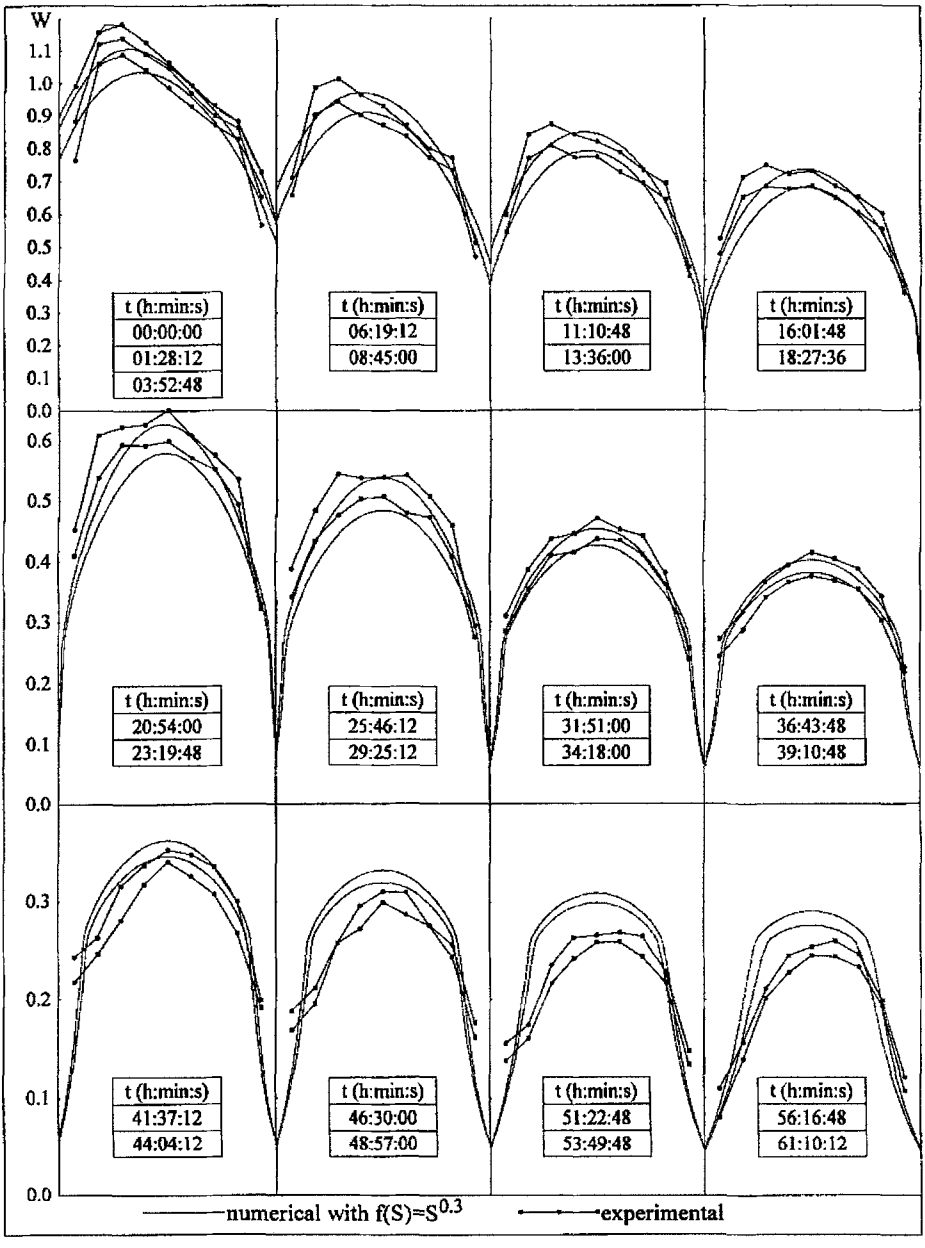

Figure 11. Adjustment of $f(S)$ from Exp. 1: comparison of experimental and predicted moisture content profiles. $L = 7\,\text{cm}$. D.C.: $T_{\text{inf}} = 70°\text{C}$; RH $= 20\%$; $\tau_T = 9.8\,\text{W m}^{-2}\,\text{K}^{-1}$; $P_{\text{inf}} = P_{\text{atm}}$. I.C.: $W =$ experimental profile at $t = 00{:}00{:}00$; $T = T_{\text{inf}} = 39.7°\text{C}$; $P = P_{\text{atm}}$.

case	❶	❷	❸
$k_{rl}(S)$	Equation (27) $f(S) = S^{0.3}$	if $S > S_{irr}$, $k_{rl} = \{(S - S_{irr})/(1 - S_{irr})\}^3$ if $S \leq S_{irr}$, $k_{rl} = 0$	S^3
$k_{rg}(S)$	Equation (28a) $f(S) = S^{0.3}$	if $S > S_{irr}$, $k_{rg} = \{(1 - S)/(1 - S_{irr})\}^3$ if $S \leq S_{irr}$, $k_{rg} = 1$	$(1-S)^3$

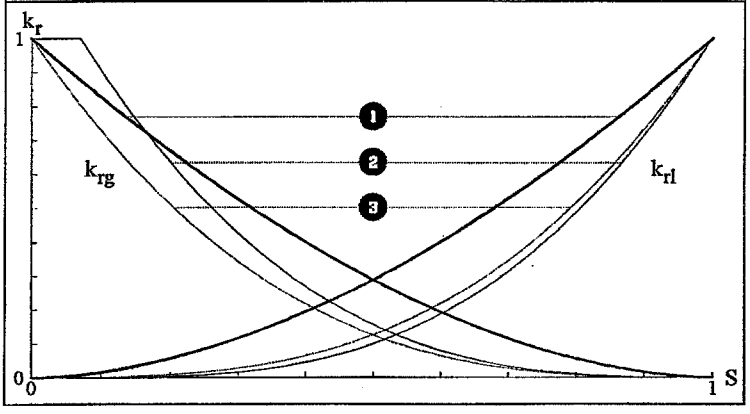

Figure 12. Comparison of the proposed relative permeability relations for sapwood of pine (case 1) to classical relations (cases 2 and 3).

This study is achieved by examining the sensitivity of liquid velocity and moisture content distributions in the variation of the relative permeabilities. In addition to the relations given by Equations {(27); (28a); $f(S) = 1$} and {(27); (28b); $f(S) = 1$}, four other forms are chosen according to the functional forms described by Equations (16) to simulate the convective drying of the sapwood of pine (i.e. the example (a) in Figure 5). The six relations ($k_{rl}(S)$, $k_{rg}(S)$) are listed and graphically represented in Figure 6. The other transport parameters and correlating functions are taken from (Bonneau, 1991) (see Appendixes A and B). The one-dimensional code used in this work (Couture *et al.*, 1995) is based on the relevant description given by Equation (5). The restrictive assumptions for the liquid velocity made in the above section, in order to explain the approach which leads us to link relative permeabilities to capillary pressure, are not adopted for this investigation. For the six test cases, the liquid velocity is calculated as indicated in Appendix C for two locations in the medium. Comparisons of the liquid velocity-moisture content curves at the quarter point ($z = 3L/4$) and near the centre ($z = L/2 + \delta z/2$) are reported in Figure 7 and comparison of the moisture content profiles in distance at equivalent times (every two hours) in Figure 8.

First of all, except in the initial transient period of the drying, the predicted liquid velocity and moisture content values for case 3 are similar to that of case 4. Since these two cases differ only by the choice of the gas phase relative permeability (see Figure 6) and because the criterion $\mathbf{P}^3$ focuses the discussion after the initial

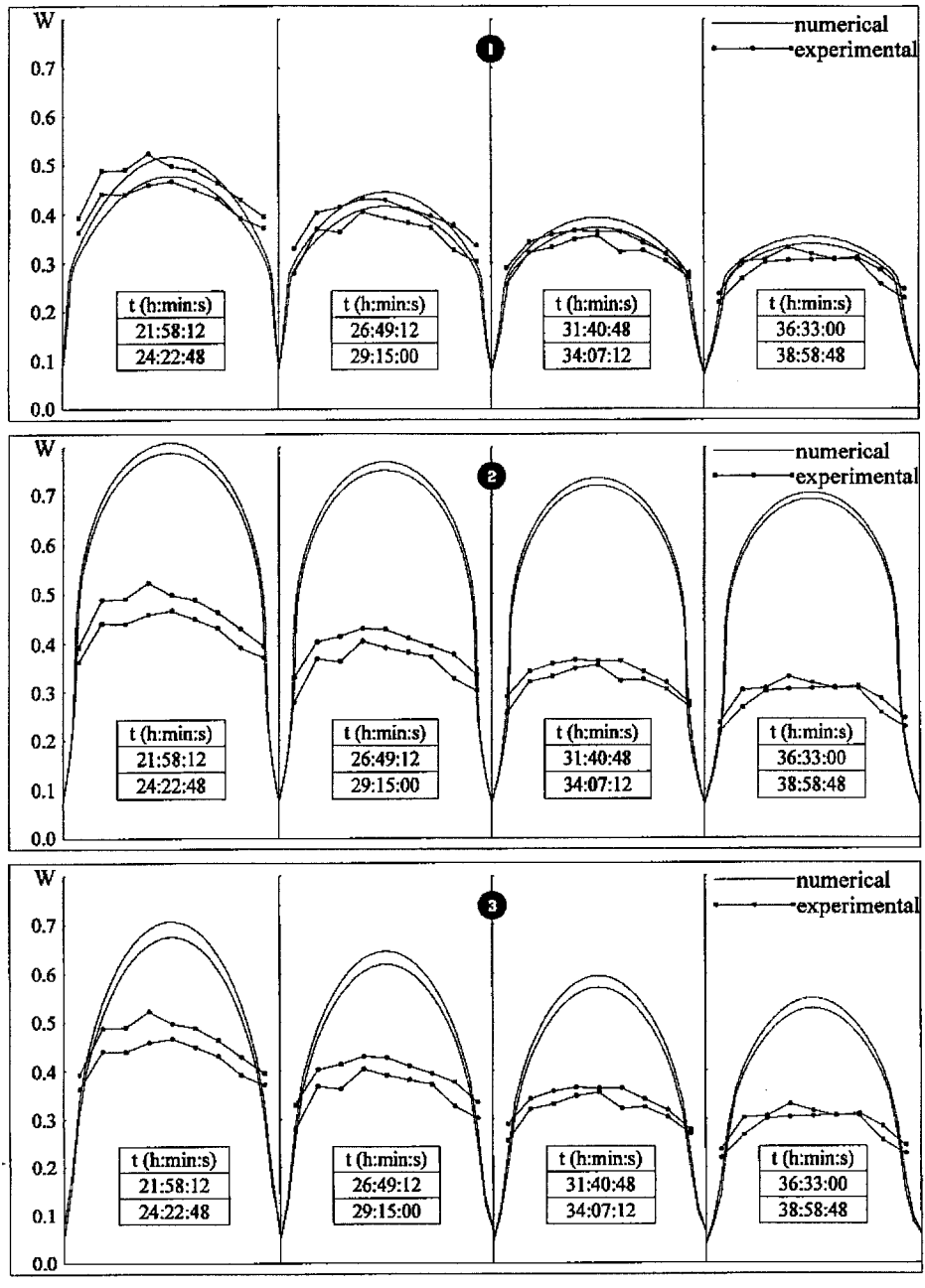

Figure 13. From Exp. 2, comparison of experimental and predicted moisture content profiles by using the relative permeability relations determined from Exp. 1 (case 1) and classical relations (cases 2 and 3). Relations are given in Figure 12. $L = 7$ cm. D.C.: $T_{\text{inf}} = 60°\text{C}$; RH = 30%; $\tau_T = 16.52\,\text{W m}^{-2}\,\text{K}^{-1}$; $P_{\text{inf}} = P_{\text{atm}}$. I.C.: W = experimental profile at t = 00:00:00; $T = T_{\text{inf}} = 41.6°\text{C}$; $P = P_{\text{atm}}$.

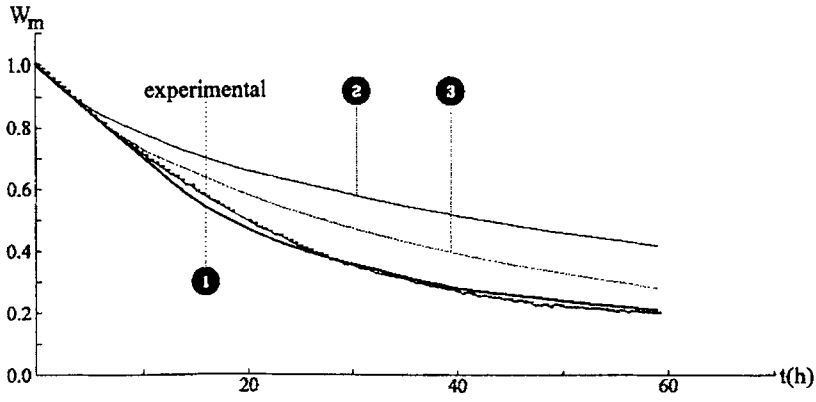

Figure 14. From Exp. 2, comparison of experimental and predicted drying kinetics by using the relative permeability relations determined from Exp. 1 (case 1) and classical relations (cases 2 and 3). Relations are given in Figure 12. $L = 7$ cm. D.C.: $T_{\text{inf}} = 60°\text{C}$; RH = 30%; $\tau_T = 16.52\,\text{W m}^{-2}\,\text{K}^{-1}$; $P_{\text{inf}} = P_{\text{atm}}$. I.C.: W = experimental profile at t = 00:00:00; $T = T_{\text{infh}} = 41.6°\text{C}$; $P = P_{\text{atm}}$.

period, one can conclude that within the framework of this study, only the k_{rl} relations have a substantial effect on the behaviour of the liquid velocity. The curves obtained for cases 1 and 2 display similar characteristics. Inconsistent with property $\mathbf{P}^3$, the liquid velocity increases as the latter stages of the nonhygroscopic region are reached and the moisture content profiles are flattening in an unrealistic way for pine wood with increasing time during the constant rate period. One can note that these behaviours are more pronounced for case 1 than for case 2, *i.e.* for the highest values of the liquid relative permeability (Figure 6). On the other hand the results for cases 5 and 6 are nearly as expected, with the liquid velocity decreasing with decreasing moisture content and the profiles showing a parabolic shape which increases in magnitude during the overall constant rate period. However, the following uncharacteristic phenomena can be observed from Figure 7(a):

- for case 5, a smooth rise of the liquid velocity appears for moisture contents between 0.75–0.45;
- for case 6, a change in slope at the end of the nonhygroscopic region leads to a non-zero value for the liquid velocity.

For cases 3 and 4, the liquid velocity either remains constant during the overall nonhygroscopic region (Figure 7(a)) or at least flattens out in the latter stages of this region (Figure 7(b)). Moreover, the profiles evolve throughout the constant rate period with a constant curvature (Figure 6). Hence, these cases appear to

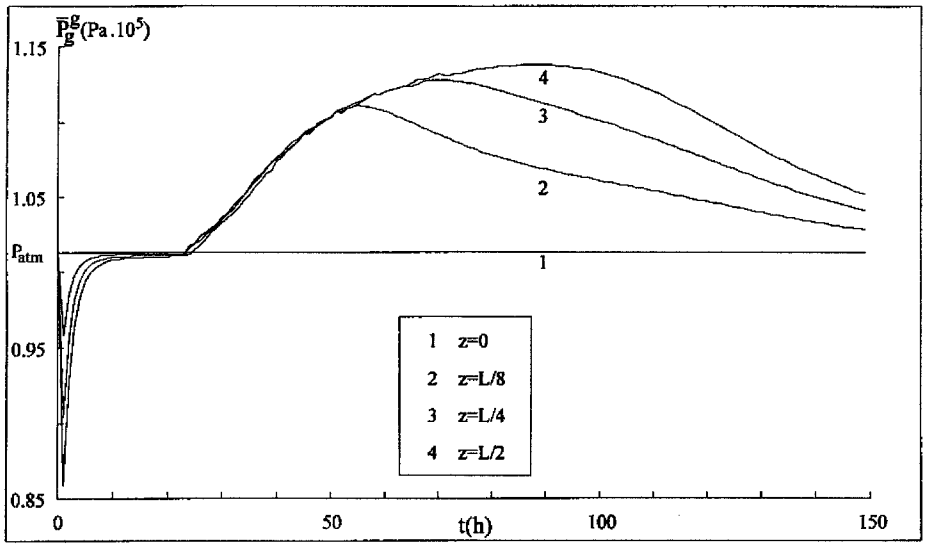

Figure 15. Predicted pressure kinetics for various locations in the medium by using the proposed relative permeability relations for sapwood of pine. $L = 7$ cm. D.C.: $T_{inf} = 70°C$; RH = 20%; $\tau_T = 9.8\,W\,m^{-2}\,K^{-1}$; $P_{inf} = P_{atm}$. I.C.: $W = 1.2$; $T = 25°C$; $P = P_{atm}$.

be a limit between the two types of behaviour described above (cases 1, 2 and cases 5, 6).

As a result of the previous observations, it can be concluded that in order to numerically predict an evolution of the liquid velocity within acceptable physical limits (property $\mathbf{P^3a}$), the relation introduced in the model for k_{rl} should provide values less than those given by relation (27) and $f(S) = 1$ (shaded area in Figure 6). This can be achieved by imposing the constraint that for whatever the value of S, $f(S)$ remains lower than one. This condition preserves property $\mathbf{P^1}$ previously observed in the relative permeability curves obtained with $f(S) = 1$ (see Figure 5), except that $f(S)$ must tend toward one as S approaches one to ensure that at this level, one and zero are the limits of k_{rl} and k_{rg}, respectively (Equations (17b) and (18b) of property $\mathbf{P^1c}$). Finally, by adding Equation (25) concerning property $\mathbf{P^3b}$, Equations (17a) and (18a) of property $\mathbf{P^1c}$ are strengthened. Thus, if a factor $f(S)$ which satisfies

$$0 < f(S) < 1; \quad \lim_{S \to 0} f(S) = 0; \quad \lim_{S \to 1} f(S) = 1, \tag{29}$$

is used in Equations (27) and (28), relative permeability relations consistent with properties $\mathbf{P^1}$ and $\mathbf{P^3}$ under the hypothesis $\mathbf{P^2}$ result.

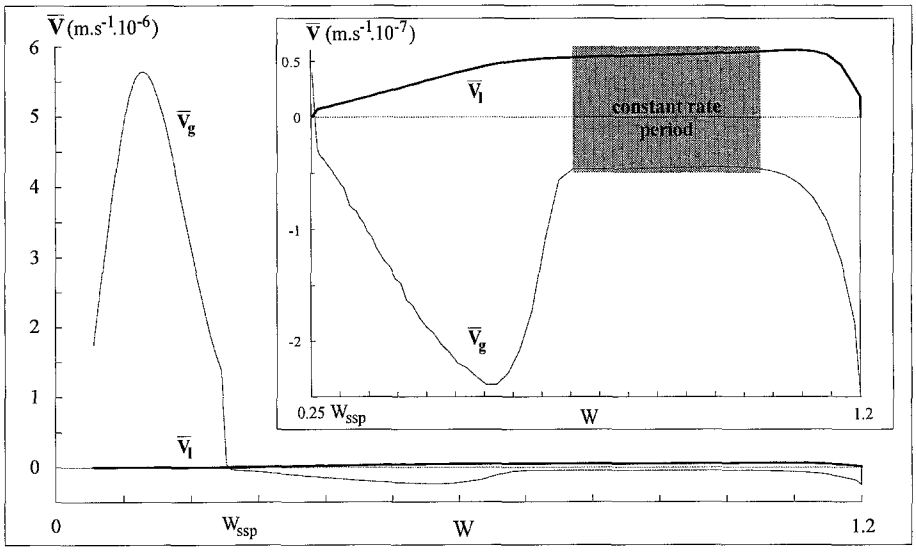

Figure 16. Predicted liquid and gas velocities versus moisture content curves at the quarter ($z = 3L/4$) of the medium by using the proposed relative permeability relations for sapwood of pine. $L = 7$ cm. D.C.: $T_{inf} = 70°C$; RH $= 20\%$; $\tau_T = 9.8\,\mathrm{W\,m^{-2}\,K^{-1}}$; $P_{inf} = P_{atm}$. I.C.: $W = 1.2$; $T = 25°C$; $P = P_{atm}$.

At this stage, it remains to determine experimentally $f(S)$. Given the dependence of the moisture content distribution on k_{rl} shown in Figure 8, one way to determine the function $f(S)$ is by calibrating the prediction of the drying model against experimental results, since the moisture content profiles can be produced experimentally with some confidence.

2.4. PROPOSED METHODOLOGY

To sum up, the following methodology is proposed to estimate the relative permeability relations.

Experimental component

(a) Measure the capillary pressure-saturation curve.
(b) Measure the moisture content (or saturation) profiles during low or middle temperature convective drying.

Numerical component

(c) Compute the moisture content (or saturation) profiles by using Equations (27) and {(28a) or (28b)} for the relative permeabilities. Compare these numerical results to the measured values in order to calibrate $f(S)$ in the range defined by Equations (29).

In the last part of this paper, the above method is applied to sapwood of pine.

3. Application

The goal of this application is to show that by fitting $f(S)$, a general evolution of the moisture distribution similar to the one determined experimentally can be predicted numerically. The material studied is sapwood of pine. As capillary pressure has been measured in the past by Bonneau (1991), only the moisture content profiles had to be obtained for this work.

3.1. MEASURES OF THE MOISTURE CONTENT PROFILES: EXPERIMENTAL SET-UP

The experimental set-up which is illustrated in Figure 9(a), consists of a heated wind tunnel supplying hot air to a sample of pine wood. During the overall drying, local moisture contents are measured using gamma attenuation (Plumb *et al.*, 1985; Collignan, 1988; Bonneau, 1991). A 450 mCi^{241} Am-source and a NaI scintillating crystal mounted to a photo multiplier tube are placed either side of the tunnel. The source and the detector are mounted on a common bidimensional moving frame (see Figure 9(b)). By allowing measures in several vertical sections of the porous slab and at regular time intervals which can be short, this system is well-adapted for determining a good estimate of the factor $f(S)$. Moreover, the wood is weighed throughout the drying process so that the global drying kinetic (evolution in time of the total moisture content removed from the sample) can be produced.

For the experiments presented here, samples come from the same plank, their thickness is 7 cm, their length and their width being 25 cm and 8 cm respectively. In order to ensure one-dimensional mass transfer, only the up and down surfaces are exposed to the drying air, the other being isolated by an adequate glue. The local moisture content has been measured for five vertical sections, with nine points regularly spaced by sections. In order to avoid end-piece effects, the considered results are those obtained for the section located at the centre (one profile every 30 minutes).

3.2. ESTIMATION OF $f(S)$

In order to run the numerical program with initial conditions corresponding as closely as possible to experimental conditions, a measured moisture content profile in distance is used to initialise the code. As the local temperatures have not been measured, this profile is chosen during the constant rate period so that the initial numerical temperature is assumed constant throughout at the wet bulb temperature. The mass transfer and heat transfer coefficients τ_m and τ_T are determined from the constant rate period identified on the drying kinetics.

The simulations are performed by using relations (27) and (28a) for the liquid and gas phase relative permeabilities, respectively. The factor $f(S)$ is based on a

simple power law form according to the constraints imposed by Equations (29) as follows

$$f(S) = S^{\gamma} \quad \text{with} \quad 0 < \gamma \leqslant 1. \tag{30}$$

The exponent γ is adjusted from a first experiment which will be called Exp. 1. Different values have been tested and the best agreement with experimental moisture content profiles (see Figure 11) together with global drying kinetics (see Figure 10) is obtained by using $\gamma = 0.3$. Nevertheless, Figure 11 indicates clearly that although a good match is provided during the overall constant rate period, it begins to decay slowly once the surfaces reach the hygroscopic region: moisture contents are overestimated below the solid saturation point. This fact is certainly not due to relative permeabilities which are constant at this stage ($k_{rl} = 0$, $k_{rg} = 1$), but can be attributed rather to the following points.

- As previously mentioned, the effective diffusivity coefficient of vapour in the medium depends on an arbitrary factor B_f. The choice of this factor can have a substantial effect in the hygroscopic region.
- The correlating function used for the effective mass diffusivity coefficient of the bound water D_b is deduced from experimental data obtained for moisture contents between 0 and 0.15. However, because the solid saturation point is about 0.3, the relation is extended arbitrarily to this value for the simulations.
- The uncertainty in moisture content measurements using gamma attenuation becomes greater for low values (Plumb *et al.*, 1985). Moreover, Collignan (1988) compared cutting and gamma methods. The same results are obtained at high humidity levels. However, gamma attenuation leads to underestimated values in the hygroscopic region. The author explains this by a change of the absorption coefficient of the water around and below the solid saturation point.

3.3. DISCUSSION

The validity of the above determined expressions for the relative permeabilities is analysed for a second experiment. Call it Exp. 2. The only difference from Exp. 1 is the drying conditions. The experimental curves are compared with the curves calculated numerically by using three couples $(k_{rl}(S), k_{rg}(S))$:

Case 1: proposed relations with $f(S) = S^{0.3}$;
Case 2: relations used by Bonneau (1991) for the same material and which take into account the irreducible saturation concept;
Case 3: extension of case 2 by ruling out the irreducible saturation concept.

The graphical representations of these relations are provided in Figure 12. Comparison of experimental and predicted drying kinetics for the three cases is shown in

Figure 14. Concerning profiles in distance, only the more interesting period, *i.e.* for experimental moisture content varying around the range [$W_{irr} \approx 0.4$, $W_{ssp} \approx 0.3$], is reported in Figure 13. The Figures 13 and 14 show that the lower liquid relative permeabilities (cases 2 and 3) predict a slower drying rate than those measured, because they induce liquid velocity which is too small. On the other hand, although drying conditions have changed, a good match with experiment remains for case 1. The important conclusion which can be drawn is that the factor $f(S)$ seems to be an intrinsic parameter of the medium.

The last point examined in this work concerns how liquid and gas velocities behave by using the relative permeabilities which have been proposed for sapwood of pine. In order to illustrate these behaviours during a complete drying process, *i.e.* including the initial transient thermal regime, the numerical code is run under the external drying conditions of Exp. 1, but with new initial conditions. Figure 15 provides some confidence in the relation proposed for the gas relative permeability. Indeed, it is obvious from the pressure profiles in time for various locations in the medium that the agreement with the classical results obtained for pine wood convective drying is highly satisfactory. The resulting gas velocity, together with the liquid velocity, are exhibited in Figure 16. The liquid velocity is, as expected, decreasing constantly toward zero during the overall nonhygroscopic region (property $\mathbf{P}^3$ introduced in part 2.1.). Moreover, according with the results obtained by Quintard and Puiggali (1986), liquid and gas velocities have unlike signs and the same amplitude during the constant rate period.

4. Conclusions

For most capillary porous media, relative permeabilities associated with two coexistent immiscible fluids such as water and humid air are not measurable directly. The numerical investigation, undertaken within the framework of a commonly used drying model, has shown the substantial effects that these parameters can have on the simulations. From this study, an approach to obtain pertinent relations has been proposed. Relative permeabilities of the liquid phase (k_{rl}) and of the gas phase (k_{rg}) were investigated using the following form:

$$k_{rl}(S) = f(S)\left(\min_{S<s<1}\left|\frac{\partial P_c}{\partial S}(s)\right| \Big/ \left|\frac{\partial P_c}{\partial S}(S)\right|\right),$$

$$k_{rg}(S) = f(1-S)\frac{\min_{S<s<1}\left|\frac{\partial P_c}{\partial S}(s)\right|}{\left|\frac{\partial P_c}{\partial S}(S_{\min} - S)\right|}$$

or

$$k_{rg}(S) = f(1-S)\frac{\min_{S<s<1}\left|\frac{\partial P_c}{\partial S}(s)\right|}{\left|\frac{\partial P_c}{\partial S}(S_{\min}(1-k_{rl}(S)))\right|},$$

with $0 < f(S) < 1$; $\lim_{S\to 0} f(S) = 0$; $\lim_{S\to 1} f(S) = 1$, $S_{\min}$ being defined by

$$\left|\frac{\partial P_c}{\partial S}(S_{\min})\right| = \min_{S<s<1}\left|\frac{\partial P_c}{\partial S}(s)\right|,$$

and the intrinsic parameter $f(S)$ calibrated by matching calculated and experimental moisture content (or saturation) distributions. In the previous formula, S is the saturation and P_c the capillary pressure.

The main advantages of this approach are summarised as follows:

- relative permeabilities are linked to the capillary pressure which is a well measurable quantity,
- the relations obtained ensure a valid behaviour for the liquid velocity,
- the irreducible saturation concept is overcome in so far as the relations which are produced provide a close representation of reality.

However, although first applications of this technique seem promising (pine wood), it would be useful to validate the method by using a more ideal medium (e.g. glass beds or sand layer):

- numerical and experimental problems due to heterogeneous and hygroscopic properties of a medium such as pine wood should be avoided,
- the relations obtained could be compared with those given by classical geometrical considerations.

Appendix A. Capillary Pressure Functions for Various Types of Pine Wood

Heartwood		*Sapwood*	
$P_c = (aS\exp(-bS) + c(1-S)S^{-d})(1 - 2.79\cdot 10^{-3}(\bar{T} - 273.16))\cdot 10^5\,\text{Pa}$			
$a = 12.12$	$b = 5.939$	$a = 1.937$	$b = 3.785$
$c = 0.046$	$d = 3.700$	$c = 0.093$	$d = 1.400$
Late wood			
$P_c = a(1-S)(\exp(bS) + cS^{-d})(1 - 2.79\cdot 10^{-3}(\bar{T} - 273.16))\cdot 10^5\,\text{Pa}$			
$a = 0.236$	$b = 3.159$	$c = 1.147$	$d = 0.620$

Appendix B. Correlating Functions for Heartwood and Sapwood of Pine used in the Simulations

	Heartwood	*Sapwood*
ε	0.5	0.615
$\bar{\rho}_s$	600	476
k	2×10^{-16}	4×10^{-16}
S_{irr}	$0.25 (\Leftrightarrow W_{\text{irr}} \approx 0.5)$	$0.07 (\Leftrightarrow W_{\text{irr}} \approx 0.4)$
Cp_s	1400	
W_{ssp}	$0.32\text{-}0.001(\bar{T} - 273.16)$	
a_w	if $W > W_{\text{ssp}}, 1$; else $\exp(-AB^{100\,\text{W}} + C)$ with:	
	$A = -2.86 \times 10^{-5}\bar{T}^2 - 1.07 \times 10^{-2}\bar{T} + 10.24$;	
	$B = -5.41 \times 10^{-4}\bar{T} + 1.01$;	
	$C = 4.97 \times 10^{-6}\bar{T}^2 - 2.67 \times 10^{-2}\bar{T} + 0.35$	
D_v^{eff}	$B_f(8.92 \times 10^{-5}\bar{T}^{1.81}/\bar{P}_g^g)$ with $B_f = \varepsilon^6$	
D_b	if $W > W_{\text{spp}}, 0$;	
	else $\exp[(11.954 - 2590.1/\bar{T})W - 1046.63/\bar{T} - 12.35]/\bar{\rho}_s$	
λ	$6 \times 10^{-4}\bar{\rho}_s(1 + W)/(1 + rv) - 0.166$ with:	
	if $W > W_{\text{ssp}}, rv = 0.15$; else $rv = 0.44\,W$	

Appendix C. Estimate of the Liquid and Gas Velocities at the Centre of the Cell $[i, i+1]$

As the space discretisation is performed by a finite element method, the code provides the values of the unknown variables at the nodes of the grid. However, in order to accurately take into account the influence of the driving gradients, the liquid velocity is evaluated at the centre of the cells. The space step is noted δz. The value of any physical quantity φ at the grid point i is named φ_i. It results from Darcy's laws

$$\bar{\mathbf{V}}_l = v_\rho^l \frac{\partial \bar{\rho}_a}{\partial z} + v_w^l \frac{\partial W}{\partial z} + v_h^l \frac{\partial \bar{H}}{\partial z} + \mathbf{v}_g^l \quad \text{with}$$

$$v_\rho^l = \frac{k k_{rl}}{\mu_l}\left(\frac{\partial P_c}{\partial \bar{\rho}_a} - \frac{\partial \bar{P}_g^g}{\partial \bar{\rho}_a}\right); \qquad v_w^l = \frac{k k_{rl}}{\mu_l}\left(\frac{\partial P_c}{\partial W} - \frac{\partial \bar{P}_g^g}{\partial W}\right);$$

$$v_h^l = \frac{kk_{rl}}{\mu_l}\left(\frac{\partial P_c}{\partial H} - \frac{\partial \bar{P}_g^g}{\partial \bar{H}}\right); \qquad \mathbf{v}_g^l = \frac{kk_{rl}}{\mu_l}\bar{\rho}_l^l \mathbf{g}.$$

$$\bar{\mathbf{V}}_g = v_\rho^g \frac{\partial \bar{\rho}_a}{\partial z} + v_w^g \frac{\partial W}{\partial z} + v_h^g \frac{\partial \bar{H}}{\partial z} + \mathbf{v}_g^g \quad \text{with}$$

$$v_\rho^g = -\frac{kk_{rg}}{\mu_g}\frac{\partial \bar{P}_g^g}{\partial \bar{\rho}}; \qquad v_w^g = -\frac{kk_{rg}}{\mu_g}\frac{\partial \bar{P}_g^g}{\partial W};$$

$$v_h^g = -\frac{kk_{rg}}{\mu_g}\frac{\partial \bar{P}_g^g}{\partial \bar{H}}; \qquad \mathbf{v}_g^g = \frac{kk_{rg}}{\mu_g}\bar{\rho}_g^g \mathbf{g}.$$

The liquid and gas velocities at the centre of the cell $[i, i+1]$ are given by

$$\bar{\mathbf{V}}_{l_{i+1/2}} = \frac{v_{\rho i+1}^l + v_{\rho_i}^l}{2}\frac{\bar{\rho}_{a_{i+1}} - \bar{\rho}_{a_i}}{\delta z} + \frac{v_{w_{i+1}}^l + v_{w_i}^l}{2}\frac{W_{i+1} - W_i}{\delta z} + \\ + \frac{v_{h_{i+1}}^l + v_{h_i}^l}{2}\frac{\bar{H}_{i+1} - \bar{H}_i}{\delta z} + \frac{\mathbf{v}_{g_{i+1}}^l + \mathbf{v}_{g_i}^l}{2};$$

$$\bar{\mathbf{V}}_{g_{i+1/2}} = \frac{v_{\rho i+1}^g + v_{\rho_i}^g}{2}\frac{\bar{\rho}_{a_{i+1}} - \bar{\rho}_{a_i}}{\delta z} + \frac{v_{w_{i+1}}^g + v_{w_i}^g}{2}\frac{W_{i+1} - W_i}{\delta z} + \\ + \frac{v_{h_{i+1}}^g + v_{h_i}^g}{2}\frac{\bar{H}_{i+1} - \bar{H}_i}{\delta z} + \frac{\mathbf{v}_{g_{i+1}}^g + \mathbf{v}_{g_i}^g}{2}.$$

References

Bizot, H., Riou, N. and Multon, J. L., 1987: Guide pratique pour la détermination des isothermes de sorption et de l'activité de l'eau, *Science des aliments, hors serie.*

Bonneau, P., 1991: Modélisasion du séchage d'un matériau hétérogène : application à un bois de résineux, Thesis, Univ. of Bordeaux I, France.

Boukadida, N. and Ben Nasrallah, S., 1995: Two dimensional heat and mass transfer during convective drying of porous media, *Drying Technol.*, **13**(3), 661–694.

Ceaglske, N. H. and Hougen O.A., 1937: Drying granular solids, *Ind. Eng. Chem.* **29**, 805–817.

Choong, E.T., 1965: Diffusion coefficients of softwoods by steady-state and theoritical methods, *Forest Product J.* **15**(1), 21–27.

Collignan, A., 1988: Elaboration et utilisation d'une cinétique de séchage – Application au pin maritime, Thesis, Univ. of Bordeaux I, France.

Couture, F., 1995: Modélisation fine d'un problème de séchage, développement d'outils adaptés, Thesis, Univ. of Bordeaux I, France.

Couture, F., Fabrie, P. and Puiggali, J.R., 1995: An alternative choice for the drying variables leading to a mathematically and physically well described problem, *Drying Technol.* **13**(3), 519–550.

Cunningham, R. M. and Kelly, J. J., 1978: Liquid transport in drying macroporous material, presented at the *1st International Drying Symposium*, Montreal.

Ferguson, W. J. and Turner, I. W., 1994: Unstructured numerical solutions techniques applied to timber drying problems, *Proceeding of the 9th International Drying Symposium, B*, pp 719–726.

Fyhr, C. and Rasmuson, A., 1994: Numerical simulation of superheated steam drying of wood chips, *Proceeding of the 9th International Drying Symposium, B*, pp 727–734.

Gobbé, C. and Gounot, J., 1991: Temperature dependent thermal diffusivity measurements by the flash method: application to solids and liquids, *High Temperature, High Pressure* **23**, 509–515.

Hernandez, J. M., 1991: Séchage du chêne, caractérisation, procédés convectif et sous vide, Thesis, Univ. of Bordeaux I, France.

Hornapour, M., Koederitz, L. and Harvey, A. H., 1986: *Relative permeability of petroleum reservoirs*, CRC Press Inc.

Kaviany, M. and Mittal, M., 1987: Funicular state in drying of a porous slab, *Int. J. Heat and Mass Transfer* **30**(7), 1407–1418.

Kanowsy, P., 1985: Densitometric analysis of a large number of wood samples, *J. Institute of Wood Science* **4**, 145–151.

Lartigue, C. and Puiggali, J. R., 1987: Caractéristiques du pin des landes nécessaires à la compréhension des phénomènes de séchage, *Actes du second Coll. Sciences et Industrie du bois, Arbolor Ed.* **2**, 57–64.

Moyne, C., 1987: Transferts couplés chaleur-masse lors du séchage: prise en compte du mouvement de la phase gazeuse, Thesis, Nancy.

Ouelhazi, N., Arnaud, G. and Forh, J. P., 1992: A two-dimensional study of wood plank drying, the effect of gaseous pressure below boiling point, *Tranport in Porous Media* **7**, 39–61.

Perré, P., 1987a: Le séchage convectif d'un bois résineux, choix, validation et utilisation d'un modèle, Thesis, Univ. of Paris VII, France.

Perré, P., 1987b: Measurements of softwoods' permeability to air: importance upon the drying model, *Int. Comm. Heat Mass Transfer* **14**, 519–529.

Perré, P. and Degiovanni, A., 1990: Simulations par volumes finis des transferts couplés en milieu poreux anisotropes : séchage du bois à basse et à haute temperature, *Int. J. Heat and Mass Transfer* **33**(11), 2463–2478.

Perré, P. and Moyne, C., 1991: Processes related to drying : part II, use of the same model to solve transfers both in saturated and unsaturated porous media, *Drying Technol.* **9**(5), 1153–1179.

Plumb, O. A., Spolek, G. A. and Olmstead, B. A., 1985: Heat and mass transfer in wood during drying, *Int. J. Heat and Mass Transfer* **28**(9), 1669–1678.

Puiggali, J. R. and Quintard, M., 1992: Properties and simplifying assumptions for classical drying models, *Advances in Drying*, **5**, 131–147.

Quintard, M. and Puiggali, J. R., 1986: Numerical modelling of transport processes during the drying of a granular porous medium, *Heat and Technology* **2**(4), 37–57.

Quintard, M. and Whitaker, S., 1993: One- and two-equation models for transient diffusion processes in two-phase system, *Advances in Heat Transfer* **23**, 369–464.

Recan, M., 1982: Simulation numérique du comportement hydrique et thermique d'un sol nu, application à l'étude de l'évaporation par télé-détection, Thèse de Docteur-Ingénieur, I.N.P.T., Toulouse.

Rogers, J. A. and Kaviany, M., 1992: Funicular and evaporative-front regimes in convective drying of granular beds, *Int. J. Heat and Mass Transfer* **35**(2), 469–480.

Spolek, G. A. and Plumb, O. A., 1981: Capillary pressure in softwoods, *Wood Sci. Technol.* **15**, 189-199.

Stanish, M. A., Schager, G. S. and Kayihan, F., 1986: A mathematical modeling of drying for hygroscopic porous media, *AIChe J.* **32**(8), 1301–1311.

Tesoro, F. O., Kimbler, O. V. and Choong, E. T,, 1972: Determination of the relative permeability of wood to oil and water, *AIChe J.* **5**(1), 21–26.

Tesoro, F. O., Choong, E. T. and Kimbler, O. V., 1974: Relative permeability and the gross pore structure of wood, *Wood and Fiber* **6**(3), 226–236.

Tsakiroglou, C. D., and Payatakes, A. C., 1990: A new simulator of mercury porosimetry for the characterization of porous materials, *J. Colloid Interface Sci.* **137**(2), 315–339.

Turner, I. W., 1994: A study of the power density distribution generated during the combined microwave and convective drying of softwood, *Proceeding of the 9th International Drying Symposium, A*, pp 89–111.

Turner, I. W. and Bremhorst, K., 1994: An investigatio, on the effect of neglecting compressible work terms in the energy equation when simulating high temperature and pressure drying processes, *Int. Comm. Heat Mass Transfer* **21**, 661–672.

Turner, I. W. and Ilic, M., 1990: Convective drying of a consolidated slab of wet porous material including the sorption region, *Int. Comm. Heat Mass Transfer* **17**, 39–48.

Whitaker, S., 1977: Simultaneous heat, mass and momentum transfer in porous media: a theory of drying, *Advances in Heat Transfer*, Vol. 13, Academic Press, New York, pp. 119–203,

Whitaker, S., 1984: Moisture transport mechanisms during the drying of granular porous media, *Proceeding of the Fourth International Drying Symposium* **1**, 31–42.

Whitaker, S., 1991: Improved constraints for the principle of local thermal equilibrium, *Ind. Eng. Chem. Res.* **30**, 983–997.

Whitaker, S. and Chou, W. T. H., 1983–84: Drying of granular porous media – theory and experiment, *Drying Technology* **1**(1), 3–33.